Airborne Thermal Infrared Hyperspectral Imaging of Buried Objects

Marc-André Gagnon, Philippe Lagueux, Jean-Philippe Gagnon, Simon Savary, Pierre Tremblay, Vincent Farley, Éric Guyot and Martin Chamberland*
Telops, 100-2600 Saint-Jean Baptiste, Québec, QC, Canada G2E 6J5

ABSTRACT

Characterization of hazardous lands using ground-based techniques can be very challenging. For this reason, airborne surveys are often preferred. The use of thermal infrared imaging represents an interesting approach as surveys can be carried out under various illumination conditions and that the presence of buried objects typically modifies the thermal inertia of their surroundings. In addition, the burial or presence of a buried object will modify the particle size, texture, moisture and mineral content of a small region around it. All these parameters may lead to emissivity contrasts which will make thermal contrast interpretation very challenging. In order to illustrate the potential of airborne thermal infrared hyperspectral imaging for buried object characterization, various metallic objects were buried in a test site prior to an airborne survey. Airborne hyperspectral images were recorded using the targeting acquisition mode, a unique feature of the Telops Hyper-Cam Airborne system which allows recording of successive maps of the same ground area. Temperature-emissivity separation (TES) was carried out on the hyperspectral map obtained upon scene averaging. The thermodynamic temperature map estimated after TES highlights the presence of hot spots within the investigated area. Mineral mapping was carried out upon linear unmixing of the spectral emissivity datacube obtained after TES. The results show how the combination of thermal information and mineral distribution leads to a better characterization of test sites containing buried objects.

Keywords: Airborne, remote sensing, hyperspectral imaging, buried objects, thermal infrared, disturbed soils

1. INTRODUCTION

Characterization of hazardous lands containing buried objects can be very challenging. For this reason, remote sensing techniques are preferred since these are non-invasive and do not generally require installation of any particular setup. The presence of a metallic buried target typically modifies the thermal properties of the soil right above the buried object like its thermal conductivity and specific heat. For this reason, thermal infrared (TIR) remote sensing has been widely used to investigate such sites.[1-4] In this spectral range (8-12 µm), remote sensing can be easily carried out in a passive way, i.e. no need for an excitation source, since signal essentially relies on self-emission. Therefore, investigations can be carried out under various illumination conditions (day-night). Despite the obvious advantages of thermal infrared for characterizing thermal signatures, finding buried targets using this technique remains a very challenging task as detection essentially relies on indirect indications of the presence of a buried targets. Substantial work has been carried out with the aim of explaining the thermal behavior of disturbed soils as a function parameters such as the buried target depth or size.[5-6]

Buried objects typically modify the thermal inertia of their surroundings. For this reason, one of the strategies used to unveil their presence consists in studying thermal patterns as a function of time during critical periods such as sunset and sunrise. During these periods of time, ground temperature changes rapidly as a result of the presence/absence of the sun. The burial procedure will typically modify the particle size, texture, moisture and mineral content and/or distribution of a small region around the site.[6] Therefore, looking for disturbed soils indications is another approach for identifying buried object sites. However, such chemical information about the soil properties is not accessible using conventional broadband TIR imaging due to the lack of spectral information. Many materials such as minerals have unique spectral emissivity signatures which can be used to track their presence and spatial distribution. For this reason, TIR hyperspectral imaging (HSI) was successfully used to find indications of disturbed soils based on spectral information.[3-4] However, most conclusions where essentially derived from statistical analysis such as covariance and principal component analysis on the spectral radiance data. It is well known that both reflection and self-emission occur and are recorded simultaneously in the

* martin.chamberland@telops.com; phone +1-418-864-7808; fax +1-418-864-7843; www.telops.com

Detection and Sensing of Mines, Explosive Objects, and Obscured Targets XX,
edited by Steven S. Bishop, Jason C. Isaacs, Proc. of SPIE Vol. 9454, 94540K
 · doi: 10.1117/12.2177182

TIR spectral range. In order to discriminate «real» thermal contrast from emissivity contrasts, one must typically perform a so called temperature-emissivity separation (TES) in order to estimate the reflection component within the measurement. The fact that prior studies were carried out on fairly homogeneous test sites (and mineral content) likely contributes to the success of prior statistical analysis on the spectral dimension without performing TES.[3-4]

Characterization of hazardous environments using ground-based techniques is typically not the preferred approach. In such cases, investigations using airborne sensors is highly suitable as it allows surveying large areas from a safe location. In this work, a TIR HSI airborne survey was carried out on a test site comprising three (3) buried targets located in an environment in which a great variety of objects, minerals and surface roughness and ground elevations were found. In order to improve signal-to-noise conditions in the collected data, airborne acquisitions were carried out using a targeting acquisition mode, a feature unique to the Telops Hyper-Cam airborne system.[7] Temperature-emissivity separation was carried out on the data in order to locate the hottest areas within the investigated scene based on the estimated thermodynamic temperature. Comparison with the apparent radiometric temperature measurements which are obtained using conventional broadband TIR imaging systems illustrate the benefits of TIR hyperspectral imaging to account for emissivity contrasts. Mineral mapping of the investigated area was carried out using the spectral emissivity data obtained from TES. The results illustrate that a combination of thermal and spectral information bring complementary indications about the buried object location.

2. EXPERIMENTAL SECTION

2.1 Telops Hyper-Cam

The Telops Hyper-Cam is a lightweight and compact hyperspectral imaging instrument which uses Fourier transform infrared (FTIR) technology. It provides a unique combination of spatial, spectral and temporal resolution for a complete characterization of the substances being monitored. Its high performance and efficiency for ground-based characterization of gas clouds has been proven through numerous field campaigns. The Hyper-Cam features a focal plane array (FPA) detector which contains 320×256 pixels over a basic 6.4°×5.1° field of view (FOV). The spectral resolution is user-selectable up to 0.25 cm^{-1} over the 3.0 to 5.0 or 7.7 to 11.8 μm spectral range for the Hyper-Cam MW (midwave) and Hyper-Cam LW (longwave) respectively.

2.2 The Telops Hyper-Cam Airborne Platform

The ground-based Telops Hyper-Cam, MW or LW, can be readily installed on a stabilization platform (Figure 1) equipped with a global positioning system (GPS) and inertial motion unit (IMU) for geo-referencing and tracking of the aircraft movements in flight. In an FTS imaging system, signal modulation, i.e. a requirement to obtain spectral resolution, is achieved using a Michelson interferometer. Modulation intensity is recorded as a function of time (interferogram) before undergoing fast Fourier transform (FFT) and radiometric calibration. Acquiring a full interferogram typically lasts about one second. Therefore, an image-motion-compensation (IMC) mirror uses the GPS/IMU data to compensate efficiently for the aircraft movements during data acquisition. The data includes all the relevant information for orthorectification and stitching. Visible images are simultaneously recorded along with the infrared datacubes using a boresight CCD camera on the airborne platform.

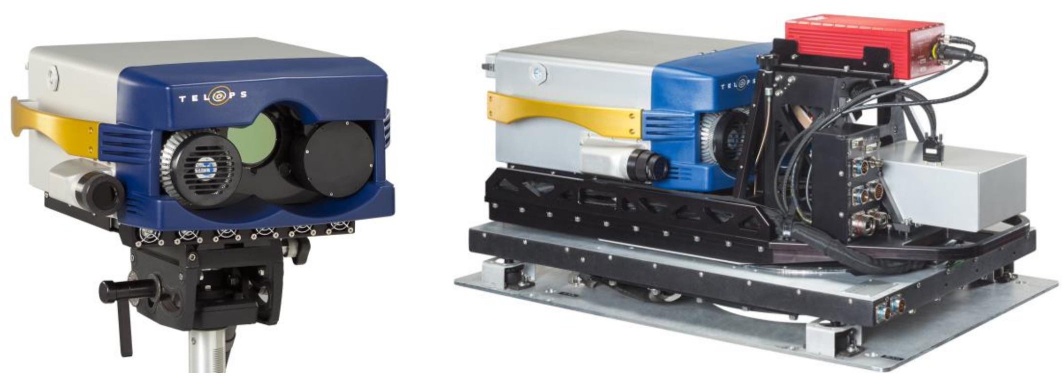

Figure 1 Telops Hyper-Cam (left) and the Hyper-Cam airborne platform (right).

2.3 Flight Conditions

The first flight was carried out using a LWIR sensor at an altitude of 2400 feet (721 meters) and a speed of 100 knots. The mean ground elevation was 15 m above sea level leading to an effective ground pixel size of 0.06 m^2/pixel. A spectral resolution of 10 cm^{-1} was used which gives a total of 49 spectral bands over the whole range covered by the FPA detector. Outside temperature and relative humidity at ground level were 23 °C and 28 % respectively.

2.4 Mapping vs Targeting Acquisition Mode

Airborne hyperspectral imaging can be carried out in two distinct acquisition modes as illustrated in Figure 2. The mapping acquisition mode is representative of most airborne sensors where individual images or datacubes, (in the case of hyperspectral sensors) are continuously recorded as the aircraft flies above its area of interest (AOI). The targeting acquisition mode takes full advantage of the IMC mirror component as it can be used to record successive hyperspectral datacubes of the same AOI, named the target area in this case. Data acquisition is typically optimized to record, depending on ground speed and altitude, as many datacubes as possible while the aircraft approaches, flies above, and beyond the target area.

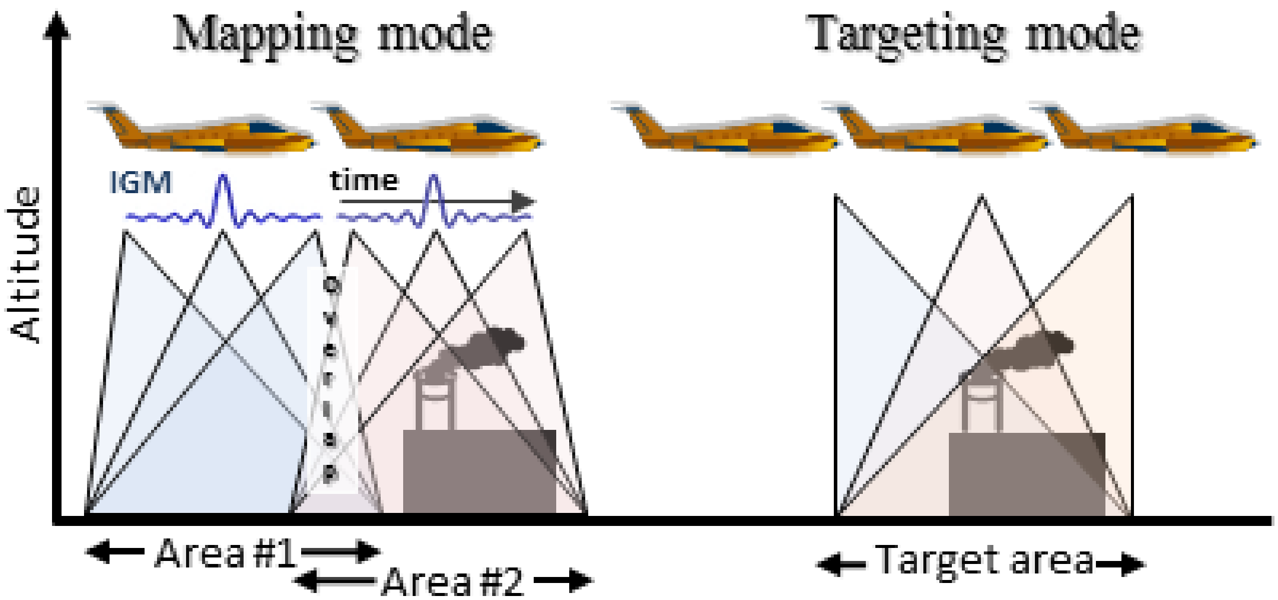

Figure 2 Mapping (left) and targeting (right) acquisition mode of the Telops Hyper-Cam airborne platform.

2.5 Data Processing

Radiometric temperature maps were obtained by computing the mean values of each pixel put on a brightness temperature scale. Temperature emissivity separation (TES) was carried out by solving Equation 1 where L is the radiance measured at the sensor level, $\varepsilon_{\bar{\nu}}$ the target spectral emissivity, Dw the effective downwelling radiance on the target, L_{target} the target's self-emission which is function of its thermodynamic temperature as described by the Planck equation, τ_{atm} is the atmospheric transmittance, and L_{atm} the radiance associated with TIR self-emission of all atmospheric components.

Equation 1 $$L = \left[L_{target}\varepsilon_{\bar{\nu}} + Dw(1-\varepsilon_{\bar{\nu}})\right]\tau_{atm} + L_{atm}(1-\tau_{atm})$$

A smoothing criterion, similar to the one described in the work of Borel [2] was used to minimize both atmospheric and downwelling radiance contributions. Radiometric temperature maps were obtained by calculating, for each pixel, the mean brightness temperature value over whole detector spectral range.

3. RESULTS AND DISCUSSION

3.1 Ground Experimental Setup

A general overview of test site prior to experiment is shown in Figure 3. It can be seen that the test site consists in a vacant area with a low vegetation coverage and a high proportion of minerals. A total of 3 burial sites were selected. Old car rims made of steel were buried in test sites #1 and #2 while a stack of aluminum plates was buried in site #3. The picture on the left in Figure 3 was recorded during the burial procedure. Target burial at site #1 and #2 was completed while site #3 still undisturbed. Yellow marker flags were placed around each target to ensure target localization in the airborne data.

Figure 3 Visible image of the 3 test sites, labeled 1 to 3, recorded from ground level during installation (left). Images recorded during burial of targets in site 1 and 2 are shown on the right. Yellow marker flags were placed on the ground in order to highlight the locations of the buried targets. Dotted lines were added to the image in order to highlight the location of the buried targets.

Each target was buried at a depth of approximately 10 cm, a full 3 days prior to that airborne survey. The soil which was removed to make some space for target each target burial was put back on top of the targets to complete the installation. As seen in Figure 4, the proportion of organic matter within the soil used to bury each target is higher than what can be found in the undisturbed areas. It should be noted that the disturbed soil areas spreads on areas much larger the target themselves.

Figure 4 Visible image of test site 1 (left), 2 (center) and 3 (right) after burial of targets recorded from ground.

3.2 TIR HSI Airborne Survey

An overview of the investigated area, collected using the boresight visible camera aboard the Telops Hyper-Cam airborne platform as well as the field-of-view (FOV) of the targeting acquisition mode, is shown in Figure 5. It can be seen that the 3 test sites are well located within the sensor FOV.

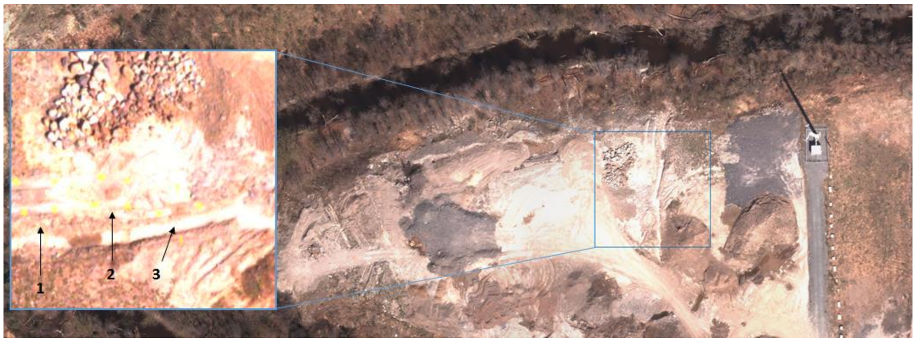

Figure 5 Visible image of the test sites recorded in flight by the boresight CCD camera of the airborne platform. The test site area is identified by a blue square. A larger picture of the test site in shown (see insert) in order to illustrate the presence of the yellow markers flags on the ground. The image saturation display was modified to enhance the presence of the yellow marker flags on the ground.

In order to investigate an area of interest (AOI) in greater details, the Telops Hyper-Cam airborne system allows successive recording of the same ground area through the means of its IMC mirror. It allows getting some time-dependent information[7] or, as in this case, improve signal-to-noise ratio by averaging multiple acquisitions. In this case, 2 successive acquisition of the test area were carried out as shown in Figure 6.

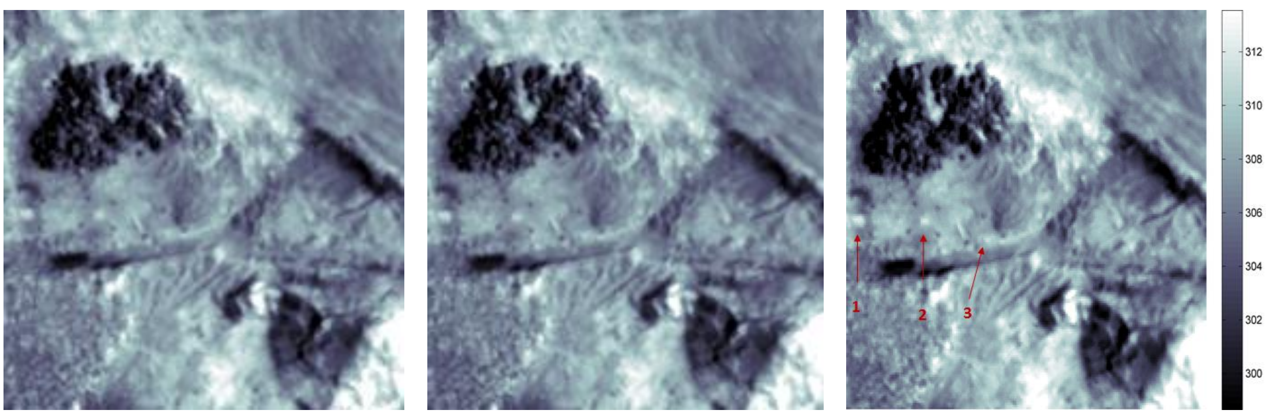

Figure 6 Temperature maps associaed with the first (left) and second (center) airborne TIR HSI acquisitions carried out on the test site. The dtacube obtained upon averaging of these 2 successive acquisition was used for data processing and its associated temperature map is presented (right). The individual test site locations were labeled for clarity purposes.

This type of result is unique to the Telops Hyper-Cam airborne system and cannot be obtained using other conventional push broom airborne systems. The targeting acquisition sequence can be visualized in order to see the dynamic information provided by this unique feature of the Telops Hyper-Cam airborne system (see Video 1). Data processing was carried out on the average scene (see Figure 6) since signal-to-noise ratio improves with scene averaging.

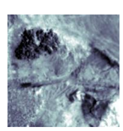

Video 1 " LWIR_targeting_buried_targets.wmv" Airborne LWIR hyperspectral imaging of the test site using the targeting acquisition mode. http://dx.doi.org/10.1117/12.2177182.1

3.3 Disturbed and undisturbed soils

The radiometric temperature map presented in Figure 6 is representative of what a conventional broadband TIR airborne sensor would measure. These temperature values are in fact apparent temperatures, i.e. of radiance equivalent to what a blackbody source would emit. However, solid materials such as minerals not only emit but also reflect thermal infrared radiation. Since the two phenomena occur simultaneously, they end-up mixed in the radiance measured at the sensor level as illustrated in Figure 7. For airborne measurements, the somewhat «cold» sky radiance is predominant within the reflection component. Consequently, low-emissivity objects will appear colder than neighbouring high-emissivity objects at the same thermodynamic temperature. Good illustrations of such phenomenon can be seen in the present case by looking at the yellow marker flags displayed on the ground. They all appear as «colder» then their immediate surroundings despite the fact that they are very thin, lie on the ground and face the same sky. In general, the emissivity of polymers (flags) is lower than minerals. From a single temperature value as provided by a broadband TIR sensor, it is not possible to discriminate cold objects from low-emissivity objects. In the investigated scene, temperature contrasts are function of both emissivity and surface self-emission. The latter is function of the «true» surface temperature, i.e. its thermodynamic temperature. Therefore, if we want to identify buried objects from thermal patterns, i.e. hot spots, one must overcome emissivity contrasts. The same comment applies for information derived from the spectral dimension. If we want to detect soil composition differences, i.e. different mineral distribution, one must overcome temperature contrasts.

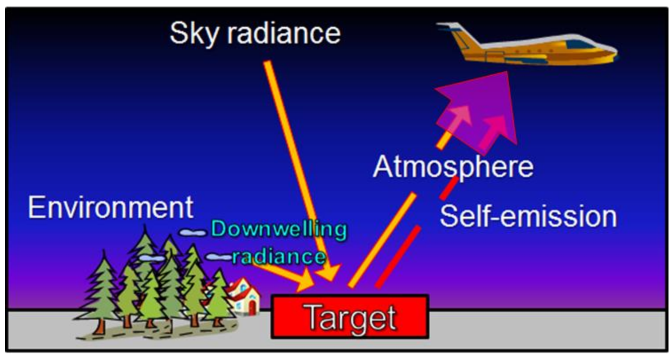

Figure 7 Airborne thermal infrared phenomenlogy illustrating the temperature-emissivity separation (TES) problematic.

The somewhat complex environment of the selected test site illustrates the challenge associated with the detection of buried objects from recognition of hot ground areas during daytime. In the present case, it would be very difficult to distinguish the test sites from other hot areas without the presence of the yellow marker flags. In order to get additional indications about the presence of buried objects, the analysis was focused on find spectral signatures associated with disturbed soils within the scene. Typical spectra associated with undisturbed soil and disturbed soil is illustrated in Figure 8.

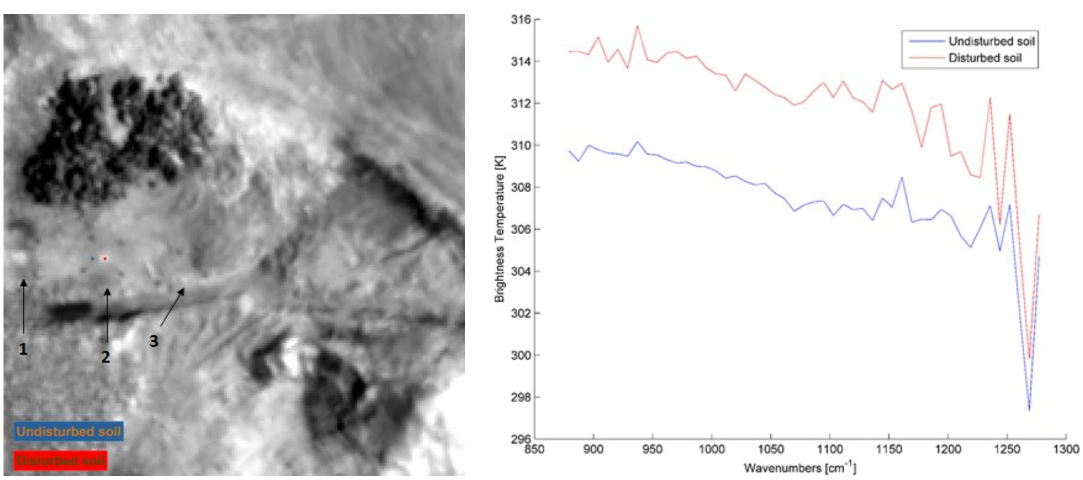

Figure 8 Selected pixels associated with disturbed and undisturbed ground surfaces (left). Their corresponding infrared spectra are shown on a brightness temperature scale (right).

As expected, the temperature measured on a disturbed soil right above a buried target is warmer than the undisturbed located soil area next to it. The series of sharp peaks above 1250 cm^{-1} is associated with atmospheric water vapor. The overall spectral patterns are also different, likely due to their different mineral composition. As seen in Figure 4, the soil brought back on top while digging a hole has a higher organic content than the top soil layer. As schematic representation of the test sites is shown in Figure 9.

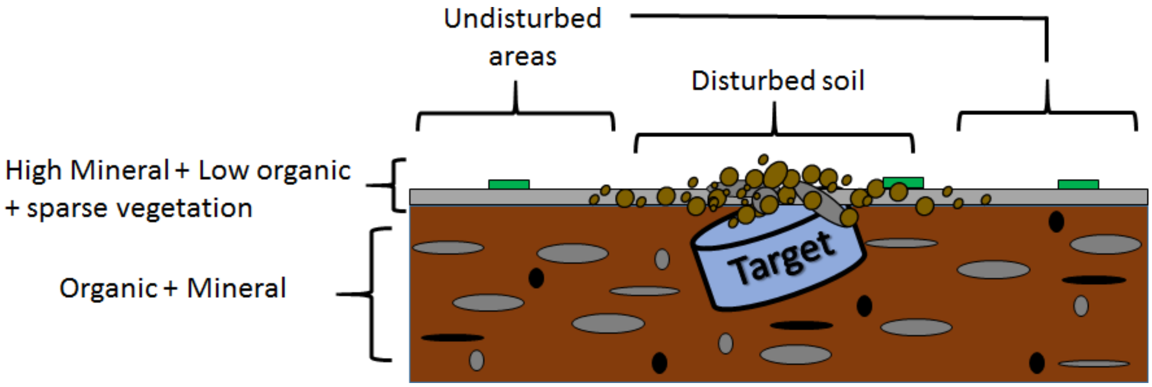

Figure 9 Schematic representation of the experimental setup.

3.4 Temperature-Emissivity Separation (TES)

Temperature-emissivity separation (TES) was carried out on a smaller AOI within the survey area as shown in Figure 10. The estimated thermodynamic temperature map obtained after TES is presented next to the corresponding radiometric temperature map for comparison purposes.

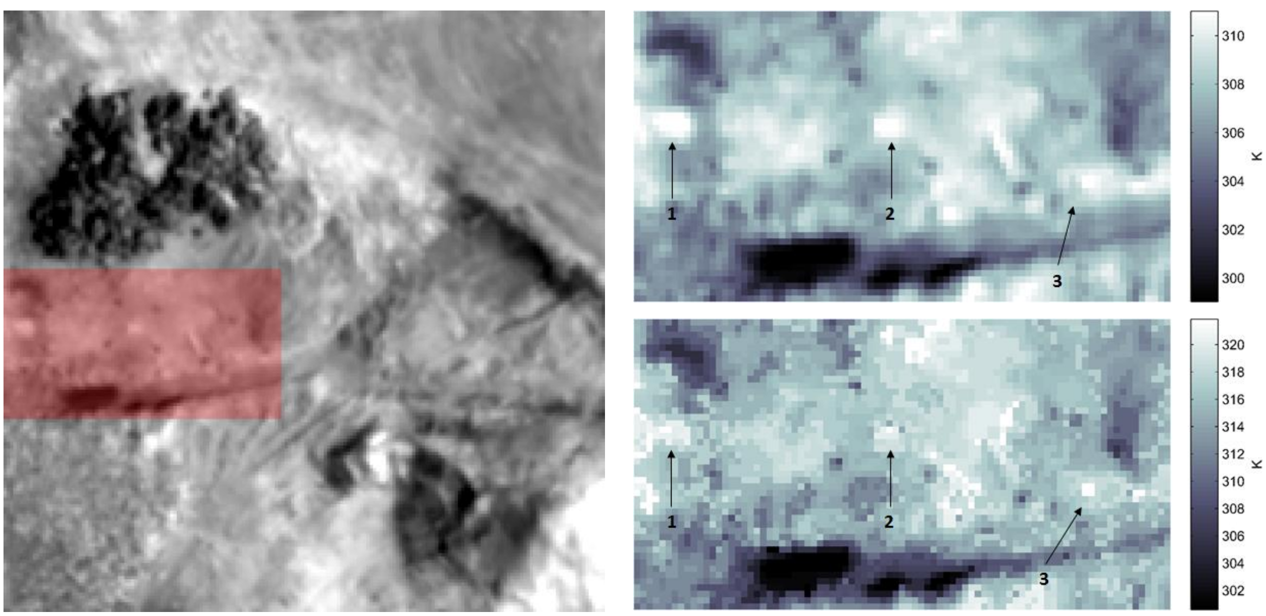

Figure 10 Area of interest (AOI) comprising the 3 buried targets on which temperature-emissivity separation (TES) was carried out is highlighted in red (left). The radiometric temperature map, i.e. apparent temperature (mean brightness temperature for each pixel), equivalent to broadband thermal imaging (top right) associated with this AOI is presented along the estimated thermodynamic surface temperature map obtained after TES (bottom right).

As expected, the estimated thermodynamic temperatures are more homogeneously distributed spatially as the TES process accounts for emissivity contrasts resulting from different ground compositions. As an example, the marker flags which could be easily located on the radiometric temperature map, due to their low emissivity, can be barely distinguished on a thermodynamic temperature contrast. In addition, the thermodynamic temperatures are systematically higher than radiometric temperature, for each pixel, due to atmospheric compensation (which is omnipresent in the broadband measurement). Despite these facts, it is still very difficult to find indications of buried targets from identifying hot ground areas. In order to highlight the hottest areas, which are at the same time the most susceptible of coinciding with buried target sites, the warmest 2 % pixels in each temperature map were identified as shown in Figure 11.

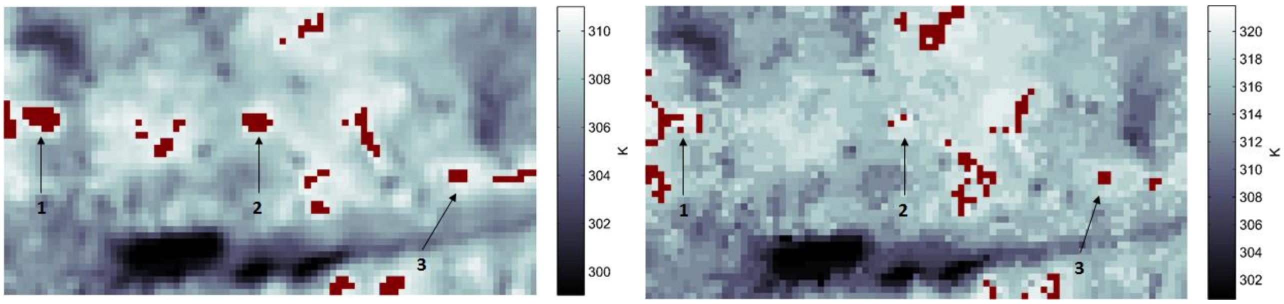

Figure 11 Two percent (2 %) fraction of hotest pixels found in the radiometric (left) and thermodynamic (right) temperature maps. The hot spots (red) are dispalyed over their corresponding temperature map for clarity purposes.

In both cases, the buried target test sites show up as part of the hottest ground areas within the scene. This results is in line with prior successful characterization of buried target sites using TIR broadband and /or hyperspectral imaging. It should be noted that the hot areas above the test sites are somewhat smaller on the thermodynamic temperature map. This could be rationalized by the fact that part of the temperature contrast observed in the radiometric temperature map comes from the disturbed soils having a different mineral composition. Under these acquisition conditions, the size of each buried object is in the order of a single (1) pixel. Therefore, their impact on the thermodynamic surface temperature is expected to be in the same order. Under both approaches, the number of suspicious sites exceed the number of test sites which indicates that more information is required to discriminate the target sites from other warm areas.

3.5 Mineral distribution

In order to look for indications of the presence of disturbed soil areas, investigation was focused on finding disparities in the mineral distribution around the test sites. In order to achieve mineral mapping, the spectral emissivity datacube must be unmixed, i.e. one must estimate the relative contributions (coefficients $A, B \ldots$) of the different components ($\varepsilon_{\overline{\nu}_n}$), associated with the different minerals, within the overall emissivity signal ($\varepsilon_{\overline{\nu}_{tot}}$). In this case, a linear mixing approach was selected as expressed in Equation 2.

Equation 2 $$\varepsilon_{\overline{\nu}_{tot}} = A\varepsilon_{\overline{\nu}_1} + B\varepsilon_{\overline{\nu}_2} + C\varepsilon_{\overline{\nu}_3} + \mathrm{D}\varepsilon_{\overline{\nu}_n}$$

Linear unmixing of the spectral emissivity data was carried out using reference spectra from commercial libraries such as John Hopkins University (JHU), Jet Propulsion Laboratory (JPL) and United State Geological Survey (USGS). Among the component list were quartz (sand), calcite, feldspar, granite and pyroxenes. The chemical maps associated with feldspar and quartz are presented in Figure 12.

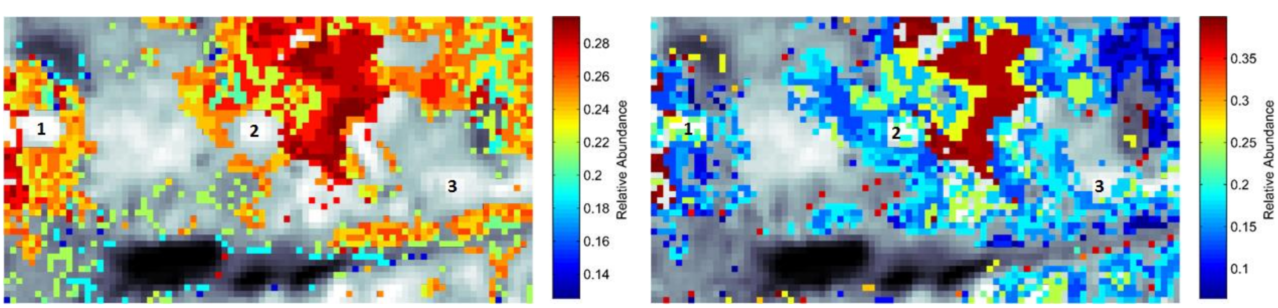

Figure 12 Mineral distribution of feldspar (left) and quartz (right) minerals obtained upon linear unmixing of the spectral emissivity datacube. The relative proportion correspond to their respective abundance coefficient in Equation 2. Chemical maps are displayed over the infrared brodband image for clarity purposes.

For all test sites, a lower contribution from the selected mineral components, to the overall spectral emissivity data, was obtained. The most reasonable explanation for such finding is that the soil used to bury the different targets has a much higher organic content than the upper most layer. Such organic material is featureless from a spectral TIR point of view, i.e. it behaves like a greybody. For this reason, the emissivity curve associated with the disturbed soils are more regular depicting less spectral features associated with minerals such as quartz and feldspar.

4. CONCLUSION

Airborne TIR HSI based on FTIR technology allows recording at high spectral and spatial resolutions. The targeting acquisition mode, unique to the Telops Hyper-Cam airborne system, allows multiple recording of successive acquisition of the same ground area, allowing signal-to-noise improvement by scene averaging. TES allows to obtain more reliable surface temperature information which is crucial to locate the presence of buried targets. The emissivity data obtained from TES provides information about the chemical nature and spatial distribution of the surface components. These two aspects provide complementary information which might help to discriminate hot spots from disturbed soils concealing buried targets.

5. REFERENCES

[1] Sendur, I. K. and Baertlein, B. A., "Techniques for improving buried mine detection in thermal IR imagery," Proc. of SPIE 3710, 1272 (1999).

[2] Nguyen, T.T., Hao, D. N., Lopez, P., Cremer, F. and Sahli H., "Thermal infrared identification of buried landmines," Proc. of SPIE 5794, 198 (2005).

[3] Shimoni, M., Perneel, C. and Gagnon, J.-P., "Detection of occluded targets using thermal imaging spectroscopy" Workshop on Hyperspectral Image and Signal Processing: Evolution in Remote Sensing (WHISPERS) 2, 1–4 (2010).

[4] McFee, J. E., Achal, S. B., Diaz, A. U. and Faust, A. A., "Comparision of broad-band and hyperspectral thermal infrared imaging of buried treat objects," Proc. of SPIE 8709, 1 (2013).

[5] Ghazali, K. H. and Jadin, M. S., "Detection improvised explosive device (IED) emplacement using infrared image" UKSim-AMSS 16th International Conference on Computer Modelling and Simulation 16, 306-309 (2014).

[6] Clayton, C. R. I., Matthews, M. C. and Simons, N. E., [Site Investigation] Wiley-Blackwell, 2nd Edition, Chapter 6 pp 1-36 (1995).

[7] Gagnon, M.-A., Tremblay, P., Savary, S., Duval, M., Farley, V. and Chamberland, M., "Airborne midwave and longwave Infrared hyperspectral imaging of gases," Proc. of SPIE 9263, 1 (2014).